

First Steps Toward Underactuated Human-Inspired Bipedal Robotic Walking

Aaron D. Ames

Abstract—This paper presents the first steps toward going from human data to formal controller design to experimental realization in the context of underactuated bipedal robots. Specifically, by studying experimental human walking data, we find that specific *outputs* of the human, i.e., functions of the kinematics, appear to be canonical to walking and are all characterized by a single function of time, termed a *human walking function*. Using the human outputs and walking function, we design a *human-inspired* controller that drives the output of the robot to the output of the human as represented by the walking function. The main result of the paper is an optimization problem that determines the parameters of this controller so as to guarantee stable underactuated walking that is as “close” as possible to human walking. This result is demonstrated through the simulation of a physical underactuated 2D bipedal robot, AMBER. Experimentally implementing this control on AMBER through “feed-forward” control, i.e., trajectory tracking, repeatedly results in 5-10 steps.

I. INTRODUCTION

The main idea behind this work is that, to achieve truly human-like robotic walking, one should first look to human walking. This deceptively simple idea is fraught with complication, as humans have highly developed neuromuscular systems which they control in highly complex ways. Yet for simple walking behaviors, such as walking on flat ground, locomotion appears to be controlled, or at least largely influenced, by central pattern generators in the spinal cord, resulting in very little cognitive load [7], [8], [9], [12], [20]. This seems to imply that there are simple patterns present in human walking which, if they can be identified, can be exploited through robotic control to achieve human-like robotic walking.

Given human walking as the motivation for achieving robotic walking, this paper begins by looking at human walking data, i.e., angles over time, achieved through motion capture of subjects walking on flat ground and at a “natural” pace. Viewing this data as the samples from a highly complex system, we seek output functions of this data (functions on the angles) that appear to characterize the system—these should be mutually exclusive, thus providing a low dimensional representation of the system’s behavior. The first result of this paper is a collection of outputs of this form. Moreover, we find that these *human outputs*, as computed from the data, appear to be described by a very simple function: the time solution to a linear spring-mass-damper system. We thus term this function the *canonical human*

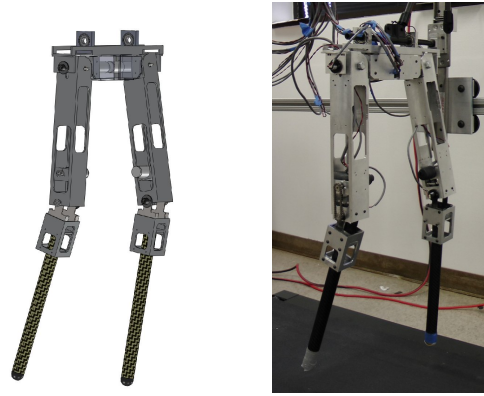


Fig. 1: Solidworks model (left) and picture of the physical bipedal robot AMBER (right), a 2D bipedal robot consisting of 5 links with underactuation at the ankle.

walking function, and we verify that in fact this function describes the human data by showing that it can be fit to the human data with a remarkably high correlation coefficient. Thus, humans appear to act like linear spring-mass-damper systems when walking on flat ground.

The simplicity that humans display when walking motivates the construction of a human-inspired controller for bipedal robots, especially in the case of underactuation where dynamic stability is necessary. In particular, using input/output linearization, we can construct an underactuated control law that drives the output of the robot to the output of the human, as represented by the canonical walking functions. Building upon [2] and [17], we characterize the zero dynamics associated with the human-inspired controller and obtain conditions on the parameters of this controller that guarantee *hybrid zero dynamics*. The problem of finding a stable walking gait is thus reduced to a 2-dimensional system and, through energy methods, the existence of a stable periodic orbit can be determined through simple inequalities. Utilizing these conditions as constraints on an optimization problem, where the cost is the least squares fit of the human walking functions to the human walking data, we obtain parameters for the human-inspired controller that result in stable underactuated robotic walking that is as close as possible to human walking.

The formal results of this paper are demonstrated on the model of a 2D underactuated bipedal robot AMBER (shown in Fig. 1). In particular, we construct a hybrid model of this system and utilize human-inspired control to obtain stable robotic walking for this biped as demonstrated through

This work is supported by NSF grants CNS-0953823 and CNS-1136104, and NHARP award 00512-0184-2009

Aaron D. Ames is with the Faculty of Mechanical Engineering, Texas A&M University, College Station, TX 77843 aames@tamu.edu

simulation. As a proof of concept, we conclude this paper by discussing the first steps toward achieving real bipedal robotic walking through the formal methods presented in this paper. The walking trajectories found through simulation are implemented on AMBER through trajectory tracking, i.e., feed-forward control, wherein the robot can repeatedly take 5-10 steps—we thereby go from human data, to formal controller design, to experimental realization.

This paper has drawn inspiration from work on dynamic robotic walking, including but not limited to: passive walking and controlled symmetries [10], [15], geometric reduction [4], [5] and hybrid zero dynamics [17], [18]. It is important to note that this is not the first paper that attempts to bridge the gap between human and robotic walking; of special note is the existing work that studies human data in the context of robotic walking, optimization and virtual constraints [14], [16], [19]; a common thread in that work is that the human data considered consists of simply the joint angles, and this data is fit with high order polynomials. The results in this paper, therefore, substantially diverge from this existing work in two important and fundamental ways: human output data is considered, and this output data is described with canonical walking functions, rather than being “overfit” by polynomials. Finally, the novelty of this paper lies in the formal extension of [2] to the case of underactuation—an extension that is much more computationally tractable than the method presented in [2] (requiring only a few minutes rather than hours) and therefore more realizable on physical robots, as evidenced by the experimental implementation results presented in this paper.

II. BIPEDAL ROBOT MODEL (AMBER)

Hybrid systems are systems that display both continuous and discrete behavior and so bipedal walkers are naturally modeled by systems of this form, with continuous dynamics when the leg swings and discrete dynamics when the foot strikes. We forgo explicitly stating the definition of a hybrid system used in this paper, along with the definition of solutions of these systems, periodic orbits and Poincaré maps, as they can be found, exactly as used in this paper, in [2]. Also note that hybrid systems, as considered here, are equivalent to systems with impulsive effects which have been well-studied in the context of bipedal robotic walking [5], [17], [18].

The formalisms of this paper are applied to the model of a physical bipedal robot: AMBER (as seen in Fig. 1). This robot has 5 links (2 calves, 2 thighs and a torso), is 61 cm tall with a total mass of 3.3 kg. AMBER is made from aluminum with carbon fiber calves, powered by 4 Maxon motors and controlled through LabView software by National Instruments. The robot has point feet, and is thus underactuated at the ankle. In addition, this robot is supported in the lateral plane via a boom; this boom does *not* provide support to the robot in the sagittal plane. Formally, we can model this robot as a hybrid system

$$\mathcal{H}\mathcal{C}_R = (X_R, U_R, S_R, \Delta_R, f_R, g_R). \quad (1)$$

The method used to construct the individual elements of this hybrid system will now be discussed.

Continuous Dynamics: The configuration space of the robot Q_R is given in coordinates by: $\theta = (\theta_{sf}, \theta_{sk}, \theta_{sh}, \theta_{nsh}, \theta_{nsk})^T$, where, as illustrated on the right, θ_{sf} is the angle of the stance foot, θ_{sk} is the angle of the stance knee, θ_{sh} is the angle of the torso with the stance thigh, θ_{nsh} is the angle of the non-stance thigh with the torso, and θ_{nsk} is the angle of the non-stance (or swing) knee. Calculating the mass and inertia properties of each link of the robot through a SolidWorks model of the robot (Fig. 1) allows for the construction of the Lagrangian:

$$L_R(\theta, \dot{\theta}) = \frac{1}{2} \dot{\theta}^T D(\theta) \dot{\theta} - V(\theta), \quad (2)$$

where $D(\theta)$ is the inertia matrix and $V(\theta)$ is the potential energy. Explicitly, this is done symbolically through the method of twists and exponential maps (see [11]). The Euler-Lagrange equations yield the equations of motion:

$$D(\theta) \ddot{\theta} + H(\theta, \dot{\theta}) = B(\theta)u.$$

Converting the equations of motion to a first order ODE yields the affine control system (f_R, g_R) :

$$f_R(\theta, \dot{\theta}) = \begin{bmatrix} \dot{\theta} \\ -D^{-1}(\theta)H(\theta, \dot{\theta}) \end{bmatrix}, \quad g_R(\theta) = \begin{bmatrix} \mathbf{0} \\ D^{-1}(\theta)B(\theta) \end{bmatrix}.$$

Since the robot is underactuated at the ankle, $U_R = \mathbb{R}^4$ and $B(\theta) \in \mathbb{R}^{5 \times 4}$.

Domain and Guard: The domain specifies the allowable configuration of the system as specified by a unilateral constraint function h_R ; for the biped considered in this paper, this function specifies that the non-stance foot must be above the ground, i.e., h_R is the height of the non-stance foot. In particular, the domain X_R is given by:

$$X_R = \{(\theta, \dot{\theta}) \in TQ_R : h_R(\theta) \geq 0\},$$

where TQ_R is the tangent space of Q_R . The guard is just the boundary of the domain with the additional assumption that the unilateral constraint is decreasing:

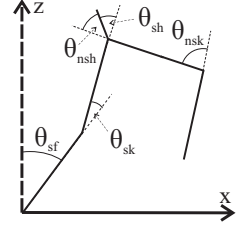
$$S_R = \{(\theta, \dot{\theta}) \in TQ_R : h_R(\theta) = 0 \text{ and } dh_R(\theta)\dot{\theta} < 0\},$$

where $dh_R(\theta)$ is the Jacobian of h_R at θ .

Discrete Dynamics. The discrete dynamics of the robot determine how the velocities of the robot change when the foot impacts the ground, while simultaneously switching the “stance” and “non-stance” legs. In particular, the reset map Δ_R is given by:

$$\Delta_R : S_R \rightarrow X_R, \quad \Delta_R(\theta, \dot{\theta}) = \begin{bmatrix} \Delta_\theta \theta \\ \Delta_{\dot{\theta}}(\theta) \dot{\theta} \end{bmatrix}, \quad (3)$$

where Δ_θ is the relabeling which switches the stance and non-stance leg at impact (by appropriately changing the angles). Here, $\Delta_{\dot{\theta}}$ determines the change in velocity due to impact; we forgo the detailed discussion on its computation, but such descriptions can be found in [2], [5] and [6].



III. HUMAN-INSPIRED CONTROL

By considering data from a human walking experiment, and looking at functions of the kinematics of the human, i.e., *human output functions*, we find that certain outputs of the human are described by the solution to a linear spring-mass-damper system which we term *canonical walking functions*. Using these outputs and their time-based representation through the canonical walking functions, we construct a human-inspired controller that drives the outputs of the robot to the outputs of the human (as represented by canonical walking functions). Moreover, we are able to make this control law autonomous through a parameterization of time based upon the position of the hip. The end result is a feedback control that is used to obtain stable underactuated bipedal robotic walking.

Human Outputs. The human walking data used in this paper was collected from 9 subjects: 2 females and 7 males with ages ranging from 17 to 30, heights ranging from 160.0 *cm* to 188.5 *cm*, and weights ranging from 47.7 *kg* to 90.9 *kg*. The subjects walked 3 meters along a line drawn on the floor at a “natural” pace, with each subject performing 11 trials. Specific details on the experiment and data analysis can be found in [2].

By studying the human walking data, the goal is to find specific outputs of the angles of a human over the course of a step, i.e., functions of the kinematics, that can be used for the purposes of robotic control. With this goal in mind, consider five outputs that appear to characterize walking in the case of the robot model and control objectives of this paper: the linearization of the x -position of the hip, p_{hip} , given by:

$$\delta p_{\text{hip}}(\theta) = L_c(-\theta_{sf}) + L_t(-\theta_{sf} - \theta_{sk}) \quad (4)$$

with L_c and L_t the length of the calf and thigh, the linearization of the slope of the non-stance leg m_{nsl} , (the tangent of the angle between the z -axis and the line on the non-stance leg connecting the ankle and hip), given by:

$$\delta m_{\text{nsl}}(\theta) = -\theta_{sf} - \theta_{sk} - \theta_{sh} - \theta_{nsh} + \frac{L_c}{L_c + L_t} \theta_{\text{nsk}}, \quad (5)$$

the angle of the stance knee, θ_{sk} , the angle of the non-stance knee, θ_{nsk} , and the angle of the torso from vertical,

$$\theta_{\text{tor}}(\theta) = \theta_{sf} + \theta_{sk} + \theta_{sh}. \quad (6)$$

These outputs were computed from the experimental human walking data for each subject, and the mean of the output data for all subjects was taken¹, with the results given in Fig. 2. Note that the motivation for considering the linearization of the position of the hip and the non-stance slope (rather than their original nonlinear formulations, as was considered in [2]) will be seen later in the paper—it allows for a simple representation of the zero dynamics especially suited to formally obtaining underactuated walking.

¹We do not normalize the human data to the parameters of AMBER because it is fairly human-like in proportions. For robots with less human-like measurements, normalization may be necessary (as was the case for NAO in [3]).

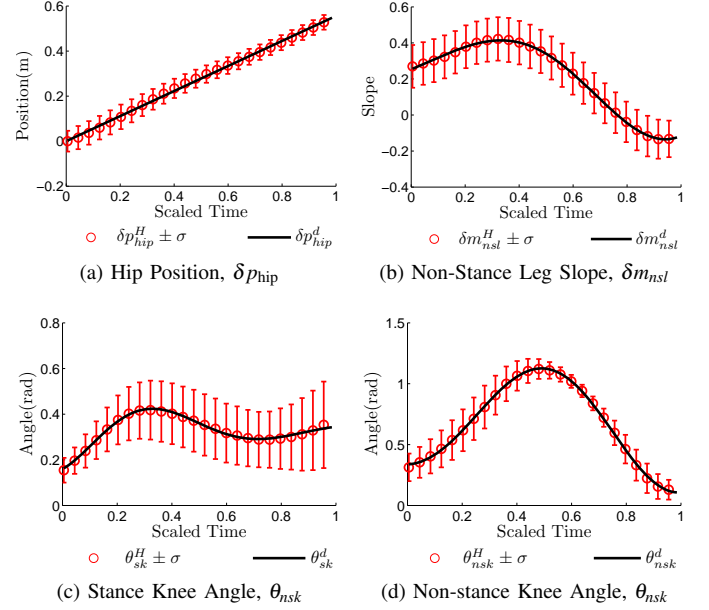


Fig. 2: The mean human output data for the nine subjects, with error bands showing one standard deviation from the mean, and the canonical walking function fits.

Human Walking Functions. The simple form that the outputs take in Fig. 2 motivates the consideration of a special class of walking functions. In particular, the linearized position of the hip appears to be essentially a linear function of time:

$$\delta p_{\text{hip}}^d(t, v) = v_{\text{hip}} t. \quad (7)$$

The remaining human outputs, δm_{nsl} , θ_{sk} , θ_{nsk} , θ_{tor} appear to be described by the solution to a linear mass-spring-damper system, which motivates the definition of the *canonical human walking function*:

$$y_H(t, \alpha) := e^{-\alpha_4 t} (\alpha_1 \cos(\alpha_2 t) + \alpha_3 \sin(\alpha_2 t)) + \alpha_5. \quad (8)$$

This function can be related to the more standard form of the solution to a linear mass-spring-damper system as by setting $\alpha_1 = c_0$, $\alpha_2 = \omega_d$, $\alpha_3 = c_1$, $\alpha_4 = \zeta \omega_n$ and $\alpha_5 = g$, where ζ is the damping ratio, ω_n is the natural frequency, $\omega_d = \omega_n \sqrt{1 - \zeta^2}$ is the damped natural frequency, c_0 and c_1 are determined by the initial conditions of the system, and g is a “gravity” related constant. Performing a least squares fit of the canonical walking functions with the mean output data results in the parameters stated in Table I. The correlations, as given in the same table, show that the fitted walking functions very closely model the human output data, i.e., the chosen human walking functions appear to be, in fact, canonical. Indeed, the coefficients of correlation are all very high, ranging from 0.9862 and 0.9997. The accuracy of the fits can be seen in Fig. 2.

Output Functions. Based upon the canonical human walking functions, we define relative degree two outputs for the bipedal robot being considered. In particular, with the goal

$y_H(t) = e^{-\alpha_4 t}(\alpha_1 \cos(\alpha_2 t) + \alpha_3 \sin(\alpha_2 t)) + \alpha_5$							
Fun.	v_{hip}	α_1	α_2	α_3	α_4	α_5	Cor.
δp_{hip}	0.9337	*	*	*	*	*	0.9991
δm_{nsl}	*	0.0117	8.6591	0.1153	-2.1554	0.2419	0.9997
θ_{sk}	*	-0.1739	13.6644	0.0397	3.3222	0.3332	0.9934
θ_{nsk}	*	-0.3439	10.5728	0.0464	-0.8606	0.6812	0.9996
θ_{tor}	*	-0.0166	10.4416	-0.0033	3.2976	0.0729	0.9862

TABLE I: Table containing parameter values of the canonical human walking functions obtained from fitting the mean human data, together with the correlations of the fits.

of the robot tracking the human outputs, we consider the following actual and desired outputs:

$$y_a(\theta) = \begin{bmatrix} \delta m_{nsl}^R(\theta) \\ \theta_{sk} \\ \theta_{nsk} \\ \theta_{tor}^R(\theta) \end{bmatrix}, \quad y_d(t) = \begin{bmatrix} y_H(t, \alpha_{nsl}) \\ y_H(t, \alpha_{sk}) \\ y_H(t, \alpha_{nsk}) \\ y_H(t, \alpha_{tor}) \end{bmatrix}, \quad (9)$$

where δm_{nsl}^R and θ_{tor}^R are the functions given in (5) and (6) computed with the parameters of the robot, and y_d consists of the human walking function given in (8) with parameters specific to each output, e.g., $\alpha_{nsl} = (\alpha_{nsl,1}, \alpha_{nsl,2}, \alpha_{nsl,3}, \alpha_{nsl,4}, \alpha_{nsl,5})$, in (8), in which case the desired non-stance slope is $\delta m_{nsl}^d(t, \alpha_{nsl}) = y_H(t, \alpha_{nsl})$. The parameters of all of the outputs considered can be combined to yield a single vector: $\alpha = (v_{hip}, \alpha_{nsl}, \alpha_{nsk}, \alpha_{sk}, \alpha_{tor}) \in \mathbb{R}^{21}$.

Control Law Construction. The goal is to drive $y_a \rightarrow y_d$, i.e., to drive the outputs of the robot to the outputs of the human. Since y_d depends on time, this could be done through standard tracking control laws [13]. With a view towards robustness, we instead parameterize time in order to obtain an autonomous control law (as motivated by both the human data and the constructions in [17], [18]). Using the fact that the forward position of the hip of the human is described by $\delta p_{hip}^d(t, v_{hip}) = v_{hip}t$, i.e., for the human $t \approx \frac{\delta p_{hip}}{v_{hip}}$, define:

$$\tau(\theta) = \frac{\delta p_{hip}^R(\theta) - \delta p_{hip}^R(\theta^+)}{v_{hip}}, \quad (10)$$

where here $p_{hip}^R(\theta^+)$ is the position of the hip of the robot at the beginning of a step² with θ^+ assumed to be a point where the height of the non-stance foot is zero, i.e., $h_R(\theta^+) = 0$.

Using the parameterization of time, we define the following *human-inspired output*:

$$y(\theta) = y_a(\theta) - y_d(\tau(\theta)), \quad (11)$$

which depends on the specific choice of parameters, α , for the human walking functions. For the affine control system (f_R, g_R) associated with the robotic model (1), we define the following control law:

$$u(\theta, \dot{\theta}) = -A^{-1}(\theta, \dot{\theta}) (L_{f_R}^2 y(\theta, \dot{\theta}) + 2\varepsilon L_{f_R} y(\theta, \dot{\theta}) + \varepsilon^2 y(\theta)), \quad (12)$$

²Note that we can assume that the initial position of the human is zero, while this cannot be assumed for the robot since the initial position of the hip will depend on the specific choice of configuration variables for the robot.

with $A(\theta, \dot{\theta}) = L_{g_R} L_{f_R} y(\theta, \dot{\theta})$ the decoupling matrix and L the Lie derivative. Note that the decoupling matrix is non-singular exactly because of the choice of output functions, i.e., care was taken when defining the human outputs so that they were ‘‘mutually exclusive.’’ It follows that for a control gain $\varepsilon > 0$, the control law u renders the output exponentially stable [13]. That is, the human-inspired output $y \rightarrow 0$ exponentially at a rate of ε ; in other words, the outputs of the robot will converge to the canonical human walking functions exponentially.

Applying the feedback control law in (12) to the hybrid control system modeling the bipedal robot being considered, $\mathcal{H}\mathcal{C}_R$ as given in (1), yields a hybrid system:

$$\mathcal{H}_R^{(\alpha, \varepsilon)} = (X_R, S_R, \Delta_R, f_R^{(\alpha, \varepsilon)}), \quad (13)$$

where, X_R , S_R , and Δ_R are defined as for $\mathcal{H}\mathcal{C}_R$, and

$$f_R^{(\alpha, \varepsilon)}(\theta, \dot{\theta}) = f_R(\theta, \dot{\theta}) + g_R(\theta, \dot{\theta})u(\theta, \dot{\theta}),$$

where the dependence of $f_R^{(\alpha, \varepsilon)}$ on the vector of parameters, α , and the control gain for the input/output linearization control law, ε , has been made explicit.

IV. HUMAN-INSPIRED HYBRID ZERO DYNAMICS

The goal of this section is to find control parameters that result in *hybrid zero dynamics* (HZD) while best fitting the human walking data. The main result is that we are able to formulate an optimization problem, *only* depending on the parameters α , that guarantees HZD while simultaneously generating a stable walking gait. This optimization is demonstrated with the mean human walking data, where it is shown that surprisingly good agreement between the human outputs and robot outputs can be obtained.

Problem Statement. The goal of the human-inspired controller (12) is to drive the outputs of the robot to the outputs of the human: $y_a \rightarrow y_d$. In other words, the controller renders the *zero dynamics surface*:

$$\mathbf{Z}_\alpha = \{(\theta, \dot{\theta}) \in TQ_R : y(\theta) = \mathbf{0}, L_{f_R} y(\theta, \dot{\theta}) = \mathbf{0}\} \quad (14)$$

exponentially stable; moreover, this surface is invariant for the continuous dynamics of the hybrid system $\mathcal{H}_R^{(\alpha, \varepsilon)}$. Note that here $\mathbf{0} \in \mathbb{R}^4$ is a vector of zeros and we make the dependence of \mathbf{Z}_α on the set of parameters explicit. It is at this point that continuous systems and hybrid systems diverge: while this surface is invariant for the continuous dynamics, it is not necessarily invariant for the hybrid dynamics. In particular, the discrete impacts in the system cause the state to be ‘‘thrown’’ off of the zero dynamics surface. Therefore, a hybrid system has *hybrid zero dynamics* if the zero dynamics are invariant through impact: $\Delta_R(S_R \cap \mathbf{Z}_\alpha) \subset \mathbf{Z}_\alpha$.

From the mean human walking data (discussed in Sect. III), we obtain discrete times, $t^H[k]$, and discrete values for the human output data, $y_i^H[k]$, for $i \in \text{Output} = \{\text{hip}, \text{msl}, \text{sk}, \text{nsk}, \text{tor}\}$; for example, $y_{msl}^H[k] = \delta m_{nsl}^H[k]$. Define the following human-data-based cost function:

$$\text{Cost}_{\text{HD}}(\alpha) = \sum_{k=1}^K \sum_{i \in \text{Output}} (y_i^H[k] - y_H(t^H[k], \alpha_i))^2 \quad (15)$$

which is simply the sum of squared residuals. The goal of *human-inspired HZD* is to find parameters α^* that solve the following constrained optimization problem:

$$\begin{aligned} \alpha^* &= \underset{\alpha \in \mathbb{R}^{21}}{\operatorname{argmin}} \operatorname{Cost}_{\text{HD}}(\alpha) \\ \text{s.t. } & \Delta_R(S_R \cap \mathbf{Z}_\alpha) \subset \mathbf{Z}_\alpha \end{aligned} \quad (\text{HZD}) \quad (16)$$

with results in the least squares fit of the human walking functions to the human output data, but subject to constraints that ensure HZD. In other words, we seek to “shape” the zero dynamics surface so that it as “human-like” as possible while simultaneously being hybrid invariant. The formal goal of this section is to restate (HZD) in such a way that it can be practically solved.

Zero Dynamics. This section utilizes the fact that the human outputs were specifically chosen to be linear in order to explicitly construct the zero dynamics. In particular, we utilize the constructions in [17], reframed in the context of canonical human walking functions. Because of the specific choice of y_a in (9), we begin by picking the following representation of the zero dynamics:

$$\begin{aligned} \xi_1 &= \delta p_{\text{hip}}^R(\theta) =: c\theta \\ \xi_2 &= D(\theta)_{1,1}\dot{\theta} =: \gamma_0(\theta)\dot{\theta} \end{aligned} \quad (17)$$

where $c \in \mathbb{R}^{5 \times 1}$ is obtained from (4), and $D(\theta)_{1,1}$ is the first entry of the inertia matrix in (2). Moreover, since ξ_1 is just the linearized position of the hip, which was used to parameterize time (10), we can write $y_d(\tau(\theta)) = y_d(\xi_1)$.

Due to the fact that we considered linear output functions, we can write $y_a(\theta) = H\theta$ for $H \in \mathbb{R}^{4 \times 5}$ with full row rank. Therefore, picking the coordinates

$$\begin{aligned} \eta_1 &= y_a(\theta) = H\theta \\ \eta_2 &= L_{f_R}y_a(\theta, \dot{\theta}) = H\dot{\theta} \end{aligned} \quad (18)$$

and defining

$$\begin{aligned} \Phi(\xi_1) &= \begin{bmatrix} c \\ H \end{bmatrix}^{-1} \begin{pmatrix} \xi_1 \\ y_d(\xi_1) \end{pmatrix} \\ \Psi(\xi_1) &= \begin{bmatrix} \gamma_0(\Phi(\xi_1)) \\ H - \frac{\partial y_d(\xi_1)}{\partial \xi_1} c \end{bmatrix}^{-1} \begin{pmatrix} 1 \\ 0 \end{pmatrix} \end{aligned}$$

it follows that for $\theta = \Phi(\xi_1)$ and $\dot{\theta} = \Psi(\xi_1)\xi_2$ that $(\theta, \dot{\theta}) \in \mathbf{Z}_\alpha$. Finally, the zero dynamics evolve according to the ODE:

$$\begin{aligned} \dot{\xi}_1 &= \kappa_1(\xi_1)\xi_2 & \kappa_1(\xi_1) &:= c\Psi(\xi_1) \\ \dot{\xi}_2 &= \kappa_2(\xi_1) & \kappa_2(\xi_1) &:= \left. \frac{\partial V(\theta)}{\partial \theta_{sf}} \right|_{\theta=\Phi(\xi_1)} \end{aligned} \quad (19)$$

with V the potential energy of the robot (2).

The advantage of the zero dynamic representation introduced is that it allows for the existence and stability of a fixed point of the zero dynamics to be determined *without integrating the ODE* [17]. This is achieved by considering the energy of the zero dynamics, and in particular the potential energy. Given a point on the guard $(\theta^-, \dot{\theta}^-) \in S_R$ with its pre-impact state $(\theta^+, \dot{\theta}^+) = \Delta_R(\theta^-, \dot{\theta}^-)$, we can compute

$\xi_1^- = \delta p_{\text{hip}}^R(\theta^-)$ and $\xi_1^+ = \delta p_{\text{hip}}^R(\theta^+)$. From this, the change in ξ_2 due to this impact can be determined through:

$$\Delta_{\mathbf{Z}}(\theta^-) = \gamma_0(\theta^+)\Delta_\theta(\theta^-)\Psi(\delta p_{\text{hip}}^R(\theta^-)) \quad (20)$$

wherein $\xi_2^+ = \Delta_{\mathbf{Z}}(\theta^-)\xi_2^-$. In essence, since the hybrid zero dynamics is 2-dimensional, when considering the stability of a limit cycle in this surface the hyperplane $\xi_1 = \xi_1^-$ can be chosen as the Poincaré section. As a result, the stability of the periodic orbit can be characterized by a 1-dimensional discrete time dynamical system which updates according to $\Delta_{\mathbf{Z}}(\theta^-)$, so this constant is intricately tied to the stability of a limit cycle in the zero dynamics surface and can be fixed ahead of time by the choice of θ^- .

The potential energy of the zero dynamics (19), given by:

$$V_{\mathbf{Z}}(\xi_1) := - \int_{\xi_1^+}^{\xi_1^-} \frac{\kappa_2(\xi)}{\kappa_1(\xi)} d\xi$$

can be used to determine when the robot will take a full step in the zero dynamics surface through the constant:

$$\mathcal{D}_{\mathbf{Z}}(\theta^-) = \frac{\Delta_{\mathbf{Z}}(\theta^-)^2}{1 - \Delta_{\mathbf{Z}}(\theta^-)^2} V_{\mathbf{Z}}(\delta p_{\text{hip}}^R(\theta^-)) + V_{\mathbf{Z}}^{\max}$$

with $V_{\mathbf{Z}}^{\max} = \max_{\xi_1^+ \leq \xi \leq \xi_1^-} V_{\mathbf{Z}}(\xi)$. Specifically, if $\mathcal{D}_{\mathbf{Z}}(\theta^-) < 0$, it will imply the existence of a limit cycle in the hybrid zero dynamics surface, and if $0 < \Delta_{\mathbf{Z}}(\theta^-) < 1$, it will imply the stability of that limit cycle [17]. Before relating these ideas back to human data and human-inspired control, it is necessary to construct the point θ^- , in terms of the parameters α , that will be considered in the optimization.

Inverse Kinematics. To achieve the goal of restating (16) in a way that is independent of state variables (position and velocity), we can use the outputs and guard functions to explicitly solve for the configuration of the system $\vartheta(\alpha) \in Q_R$ on the guard in terms of the parameters. In particular, let

$$\vartheta(\alpha) = \theta \quad \text{s.t.} \quad \begin{bmatrix} y(\Delta_\theta \theta) \\ h_R(\theta) \end{bmatrix} = \begin{bmatrix} \mathbf{0} \\ 0 \end{bmatrix}, \quad (21)$$

where Δ_θ is the relabeling matrix (3). Note that $\vartheta(\alpha)$ exists because of the specific structure of the outputs, $y(\Delta_\theta \theta)$, chosen. In fact, the reason for considering y at the point $\Delta_\theta \theta$ is because this implies that the configuration at the beginning of the step is $\theta^+ = \Delta_\theta \theta$ and thus $\tau(\Delta_\theta \theta) = 0$ implying that: $y(\Delta_\theta \theta) = H\Delta_\theta \theta - y_d(0)$, or there is a solution to (21) because of the simple form that y takes at $\Delta_\theta \theta$.

Using $\vartheta(\alpha)$, we can explicitly solve for a point $(\vartheta(\alpha), \dot{\vartheta}(\alpha)) \in \mathbf{Z}_\alpha \cap S_R$ such that the velocity of the hip at that point is v_{hip} ; thus the speed of the robot can be controlled through the choice of parameters. In particular, for

$$Y(\theta) = \begin{bmatrix} d\delta p_{\text{hip}}^R(\theta) \\ dy(\theta) \end{bmatrix}, \quad (22)$$

with $d\delta p_{\text{hip}}^R(\theta)$ and $dy(\theta)$ the Jacobian of p_{hip} and y , respectively, define

$$\dot{\vartheta}(\alpha) = Y^{-1}(\vartheta(\alpha)) \begin{bmatrix} v_{\text{hip}} \\ \mathbf{0} \end{bmatrix}, \quad (23)$$

where Y is invertible because of the choice of outputs.

Main Result. We now present the main result of this paper. Using $\vartheta(\alpha)$ and $\dot{\vartheta}(\alpha)$, we can restate the optimization problem (16) in terms of only parameters of the system. Moreover, by solving the restated optimization problem, we automatically obtain an initial condition corresponding to stable periodic walking. Note that space constraints prevent the inclusion of a proof, but it essentially follows from combining the results of [17] and [2] (see [3] for an additional formal results in the case of full actuation).

Theorem 1: *The parameters α^* solving the constrained optimization problem:*

$$\alpha^* = \underset{\alpha \in \mathbb{R}^{21}}{\operatorname{argmin}} \operatorname{Cost}_{\text{HD}}(\alpha) \quad (24)$$

$$\text{s.t. } y(\vartheta(\alpha)) = \mathbf{0} \quad (C1)$$

$$dy(\Delta_\theta \vartheta(\alpha)) \Delta_\theta(\vartheta(\alpha)) \dot{\vartheta}(\alpha) = \mathbf{0} \quad (C2)$$

$$dh_R(\vartheta(\alpha)) \dot{\vartheta}(\alpha) < 0 \quad (C3)$$

$$\mathcal{D}_{\mathbf{Z}}(\vartheta(\alpha)) < 0 \quad (C4)$$

$$0 < \Delta_{\mathbf{Z}}(\vartheta(\alpha)) < 1 \quad (C5)$$

yield hybrid zero dynamics: $\Delta_R(S_R \cap \mathbf{Z}_{\alpha^*}) \subset \mathbf{Z}_{\alpha^*}$. Moreover, there exists an $\hat{\varepsilon} > 0$ such that for all $\varepsilon > \hat{\varepsilon}$ the hybrid system $\mathcal{H}_R^{(\alpha^*, \varepsilon)}$ has a stable periodic orbit with fixed point $(\theta^*, \dot{\theta}^*) \in S_R \cap \mathbf{Z}_{\alpha^*}$ given by:

$$\theta^* = \vartheta(\alpha), \quad \dot{\theta}^* = \Psi(c\vartheta(\alpha)) \left(-\sqrt{\frac{-V_{\mathbf{Z}}(\vartheta(\alpha))}{1 - \Delta_{\mathbf{Z}}(\vartheta(\alpha))}} \right).$$

V. SIMULATION, EXPERIMENTATION & CONCLUSIONS

This section applies the results of this paper, and specifically the main result, to the bipedal robot AMBER. This is done both in simulation and through experimentation. In the context of simulation, we are able to demonstrate that Theorem 1 can be effectively applied to the formal model of AMBER to obtain “human-like” robotic walking. Moreover, the walking found in simulation is implemented on the physical robot, where 5 unsupported steps were achieved; therefore, while we do not obtain sustainable robotic walking, these experimental results indicate that the formal theory appears to be practically applicable.

Simulation Results. We apply Theorem 1 to the hybrid model of AMBER $\mathcal{H}_{\mathcal{C}_R}$ using the mean human data to calculate the cost; specifically, the optimization is numerically solved in MATLAB. The end result of this optimization is a collection of control parameters for the α^* resulting in a hybrid system $\mathcal{H}_R^{(\alpha^*, \varepsilon)}$. Moreover, the same optimization automatically generates a fixed point to a stable periodic orbit; this is verified by picking $\varepsilon = 10$ and checking the eigenvalues of the linearization of the Poincaré map for which the maximum magnitude is 0.7761 (and hence less than 1). Tiles of the walking obtained in simulation can be seen in Fig. 3(e), with the periodic orbit pictured in Fig. 3(c). In 3(a),(b) the outputs of the robot (actual and desired) are compared to the human data; from this one concludes both that hybrid zero dynamics is achieved (the actual and desired outputs agree) and the outputs of the robot and the

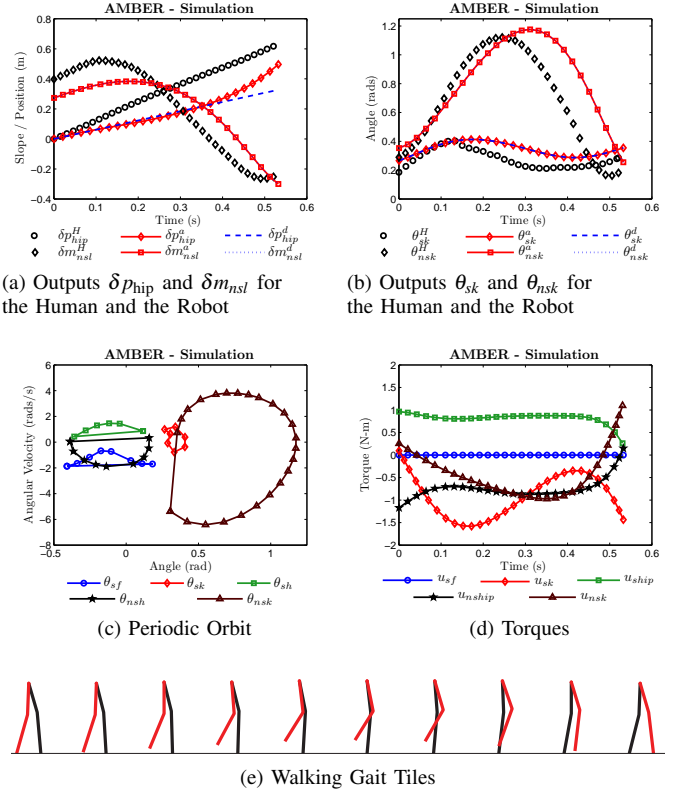


Fig. 3: Comparison of the outputs of the human and the robot during the course of a step (a),(b), the periodic orbit of the walking achieved through Theorem 1 (c), the torques during a step for the walking (d) and tiles of the walking gait.

human are surprisingly close (especially given the difference between the robot and the human, and given the fact that the robot is underactuated). Finally, the walking obtained uses very low torques for the size and weight of AMBER as can be seen in Fig. 3(d), meaning the torques are achievable by the small motors actuating AMBER.

Experimental Results. In order to provide evidence of the applicability of the theory presented in this paper, it was applied to the physical bipedal robot AMBER (see Fig. 1). The robot itself was supported in the lateral plane by a boom, but it had no support in the sagittal plane, i.e., it can fall. In addition, the robot was placed on a treadmill, with the speed of the treadmill set to the average speed of the walking found in simulation. The trajectories produced by the simulation of AMBER were exported to LabView, and a PD control loop was used to track these trajectories on the robot through the use of both relative encoders on the motor and absolute encoders on the shaft of each joint. That is, since we were only tracking the simulation trajectories on the robot, the control strategy was essentially “feed-forward.” Through these methods, we were able to obtain 5-10 steps on the robot, repeatedly over multiple experimental runs. An example of the walking behavior achieved on the robot during these “bursts” of walking can be seen in Fig. 4(c) and

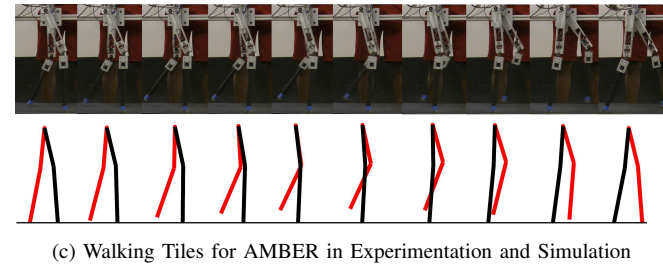
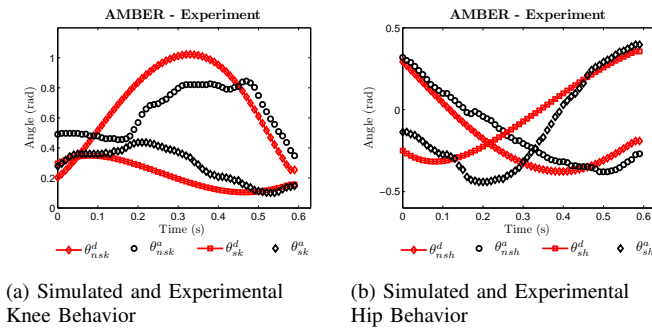


Fig. 4: Comparison of the simulated and experimental angles of AMBER over one step (a),(b) and tiles of the experimental step taken (c).

at [1], which shows snapshots of the walking on the physical robot (top) compared to snapshots of the simulated walking that generated the trajectories that were tracked by the robot (bottom). As can be seen, there is good agreement between the simulated and physical behaviors; this seems to imply that, in fact, the model of the robot and the formal methods developed in this paper are valid approximations of reality. That being said, while we were able to achieve “reasonable” tracking of the simulation trajectories, we were not able to achieve exact tracking as can be seen in Fig. 4(a),(b). We argue that this is due to the fact that trajectory tracking is inherently non-robust for systems with time sensitive behavior such as robotic walkers—we were not able to start the robot at “exactly” the same initial condition as the simulated walking (this error can be seen in Fig. 4(a),(b)), and the resulting disturbances could not be corrected through trajectory tracking. We argue that this is what resulted in the robot falling after a series of 5-10 steps, and why we were not able to achieve sustained walking.

Conclusions. This paper describes the first steps toward achieving human-inspired underactuated bipedal robotic walking, specifically going from human data to formal controller design to experimental implementation. The main contributions of this paper are formal in nature; for an underactuated bipedal robot, we find outputs of the human that are characterized by “simple” walking functions which describe the solution to a linear mass-spring-damper system, construct a control law so that the robot and the human display the same behavior in the output and, finally, present an optimization problem, stated only in terms of the control parameters, that provides the best fit of the human walking

data while simultaneously and automatically generating a stable walking gait for the bipedal robot. These formal results are demonstrated in simulation. Finally, we discuss the first steps toward applying this formal work to a physical bipedal robot, AMBER, demonstrating that through essentially feed-forward control it is possible to obtain the precursors to walking, “steps,” on the robot. Future work will be devoted to achieving sustainable walking on AMBER through these methods by implementing a feedback control strategy on the robot.

Acknowledgements. I would like to thank Shishir Nadubettu Yadukumar and Murali Krishna for their work on control implementation on AMBER, and Jordan Lack and Michael Zeagler for their work in constructing AMBER. In addition, I would like to thank the anonymous reviewers for their detailed and constructive comments on the manuscript.

REFERENCES

- [1] AMBER’s first steps toward human-inspired bipedal robotic walking. <http://www.youtube.com/watch?v=LGulnhbiFB8>.
- [2] A. D. Ames. First steps toward automatically generating bipedal robotic walking from human data. In *8th International Workshop on Robotic Motion and Control*, Poland, 2011.
- [3] A. D. Ames, E. A. Cousineau, and M. J. Powell. Dynamically stable robotic walking with NAO via human-inspired hybrid zero dynamics. In *Hybrid Systems: Computation and Control*, Beijing, 2012.
- [4] A. D. Ames, R. D. Gregg, and M. W. Spong. A geometric approach to three-dimensional hipped bipedal robotic walking. In *45th Conference on Decision and Control*, San Diego, CA, 2007.
- [5] J. W. Grizzle, C. Chevallereau, A. D. Ames, and R. W. Sinnet. 3D bipedal robotic walking: models, feedback control, and open problems. In *IFAC Symposium on Nonlinear Control Systems*, Bologna, 2010.
- [6] Y. Hürmüzli and D. B. Marghitu. Rigid body collisions of planar kinematic chains with multiple contact points. *Intl. J. of Robotics Research*, 13(1):82–92, 1994.
- [7] A. J. Ijspeert. Central pattern generators for locomotion control in animals and robots: A review. *Neural Networks*, 21(4):642–653, 2008.
- [8] O. Kiehn. Locomotor circuits in the mammalian spinal cord. *Annu Rev Neurosci.*, 29:279–306, 2006.
- [9] M. MacKay-Lyons. Central pattern generation of locomotion: A review of the evidence. *Physical Therapy*, 82(1):69–83, 2002.
- [10] T. McGeer. Passive dynamic walking. *Intl. J. of Robotics Research*, 9(2):62–82, 1990.
- [11] R. M. Murray, Zexiang Li, and S. S. Sastry. *A Mathematical Introduction to Robotic Manipulation*. CRC Press, Boca Raton, 1994.
- [12] J. B. Nielsen. How we walk: Central control of muscle activity during human walking. *Neuroscientist*, 9(3):195–204, 2003.
- [13] S. S. Sastry. *Nonlinear Systems: Analysis, Stability and Control*. Springer, New York, 1999.
- [14] A. Shiriaev, L. Freidovich, and I. Manchester. Can we make a robot ballerina perform a pirouette? Orbital stabilization of periodic motions of underactuated mechanical systems. *Annual Reviews in Control*, 32(2):200–211, 2008.
- [15] M. W. Spong and F. Bullo. Controlled symmetries and passive walking. *IEEE TAC*, 50(7):1025–1031, 2005.
- [16] S. Srinivasan, I. A. Raptis, and E. R. Westervelt. Low-dimensional sagittal plane model of normal human walking. *ASME J. of Biomechanical Eng.*, 130(5), 2008.
- [17] E. R. Westervelt, J. W. Grizzle, C. Chevallereau, J. H. Choi, and B. Morris. *Feedback Control of Dynamic Bipedal Robot Locomotion*. CRC Press, Boca Raton, 2007.
- [18] E. R. Westervelt, J. W. Grizzle, and D. E. Koditschek. Hybrid zero dynamics of planar biped walkers. *IEEE TAC*, 48(1):42–56, 2003.
- [19] Y. Xiang, J. Arora, H. J. Chung, H. J. Kwon, Salam S. Rahmatalla, R. Bhatt, and K. Abdel-Malek. Predictive simulation of human walking transitions using an optimization formulation. *Structural and Multidisciplinary Optimization*, pages 1–14.
- [20] J. F. Yang and M. Gorassini. Spinal and brain control of human walking: Implications for retraining of walking. *Neuroscientist*, 12(5):379–389, 2006.